Journal of Applied Geophysics 144 (2017) 134–143

Contents lists available at ScienceDirect

Journal of Applied Geophysics

journal homepage: www.elsevier.com/locate/jappgeo

Estimating the hydrogeological parameters of an unconfined aquifer with the time-lapse resistivity-imaging method during pumping tests: Case studies at the Pengtsuo and Dajou sites, Taiwan

Chang Ping-Yu [a,*], Chang Lian-Cheng [b], Hsu Shao-Yiu [c], Tsai Jui-Pin [b], Chen Wen-Fu [d]

[a] National Central University, Jongli, Taiwan
[b] National Chiao Tung University, Hsinchu, Taiwan
[c] National Taiwan University, Taipei, Taiwan
[d] Chia Nan University of Pharmacy and Sciences, Tainan, Taiwan

ARTICLE INFO

Article history:
Received 22 September 2016
Received in revised form 22 June 2017
Accepted 25 June 2017
Available online 11 July 2017

ABSTRACT

We conducted time-lapse resistivity imaging during pumping tests at the Pengtsuo and Dajou test sites in Taiwan in order to examine the feasibility of estimating hydrogeological parameters with resistivity variations. Core logs reveal that the subsurface consists mainly of at least 100-m-thick gravel and sand at the two test sites. The resistivity differences between the pumping stages and pre-pumping background are well correlated to water level changes that are due to the dewatering of pumping activity. Therefore, it is possible to use the geometry of resistivity anomalies to estimate the hydraulic conductivity of the unconfined aquifer using the distance-drawdown equation for pumping tests in unsaturated aquifers. For each site, we used the contours of resistivity variations and recorded water levels in the pumping well to depict the bottom of the drawdown cone. The estimated hydraulic conductivity and specific yield, respectively, are 1.33×10^{-4} m/s and 0.12 at the Pengtsuo site, and are 2.50×10^{-4} m/s and 0.22 at the Dajou site. These values are consistent with the parameters that engineers from Taiwan Sugar Company calculated previously regarding groundwater-level variations in multiple wells (9.65×10^{-5} m/s and 0.13 at Pengtsuo, and 1.00×10^{-3} m/s and 0.19 at Dajou). This consistency suggests that resistivity imaging can perhaps serve as an alternative way to yield information about hydrogeological parameters.

1. Introduction

Many groundwater researchers use pumping tests to estimate hydraulic parameters such as the hydraulic conductivity and the storage coefficients of aquifers. Many results-based estimates of hydraulic parameters have traditionally rested on both classical methods and homogeneous-interpretation models (e.g., Cooper and Jacob 1946; Theis, 1935). However, the time-varying geometry of drawdown cones associated with heterogeneous aquifers may yield varying hydraulic parameters over time in test evaluations (Leven and Dietrich, 2006). As a result, it is important to monitor this geometry when the pumping activities of pumping-test analyses cause time-varying drawdowns. Unfortunately, drilling a series of wells for the specific purpose of monitoring is as time-consuming as it is uneconomical. Aware of these issues, researchers have tried to use non-invasive geophysical methods for monitoring. For instance, Endres et al. (2000) tried to estimate the drained-water volume for various times during a pumping test with the transition zone drawdown-distance relationships derived from ground-penetrating radar (GPR) profiles. Bevan et al. (2003) used GPR to map a water table during a pumping test's dewatering and recovery phase. Rizzo et al. (2004) and Straface et al. (2007) used the self-potential responses associated with pumping and recovery tests, respectively, to estimate the hydraulic conductivity around pumping wells. Among these geophysical studies, electrical resistivity imaging (ERI) is noticeably less popular than the self-potential method and GPR for monitoring dewatering and recovery processes during pumping tests. Researchers frequently use resistivity-imaging methods in various environments to investigate subsurface structures (e.g., Binley et al., 2002; Chang et al., 2011; Kemna et al., 2002; Kim et al., 2002; Mitchell et al., 2008; Toran et al., 2010; van Schoor, 2002). Loke et al. (2013) usefully reviewed developments in a variety of resistivity surveys. Barker and Moore (1998) used the ERI method to monitor the saturation changes during a four-hour pumping test in an unconfined aquifer. They discovered that a maximum 15% change in resistivity was centered on the pumping borehole but was asymmetric around the pumping borehole. The findings in Barker and Moore (1998) suggest that the ERI method is a feasible technique for

* Corresponding author.
E-mail address: pingyuc@ncu.edu.tw (P.-Y. Chang).

http://dx.doi.org/10.1016/j.jappgeo.2017.06.014
0926-9851/

providing alternative information regarding, in particular, the geometry of the drawdown cone for pumping tests. In our current study, we have used an ERI method to examine how the geometry of the dewatering volume varies with time and different pumping rates. In addition, we have estimated the hydrogeological parameters, such as hydraulic conductivity and specific yields, at different stages with the results of time-lapse ERI surveys, and we have compared our estimates with the values calculated from the multiple-well pumping tests.

2. Pumping-test settings and ERI-survey configurations

We conducted our pumping tests at two sites: one is located near the Pengtsuo elementary school in southwestern Taiwan's Pingtung County, and the other is located near the Dajou elementary school in northeastern Taiwan's Ilan County. In both the Pengtsuo and Dajou sites, core drilling logs show that the sediment within a depth of 120 m consists of thick layers of gravel and is a component of major unconfined aquifers (Fig. 1). We conducted a pumping test in the Pengtsuo well (P1) and, in addition, installed water-level gauges in P1 and the other three Pengtsuo-based observation wells (O1, O2, and W1) to monitor groundwater levels. At the Dajou site, we conducted pumping tests in its pumping well (PD-1), and we installed water-level gauges in both that well and a single Dajou-based observation well (OD-1). Fig. 2a and b show the configurations of the wells at the Pengtsuo and Dajou sites, respectively. The pumping tests at the Pengtsuo and Dajou sites took place in three stages: the background, the stepwise-pumping, and the continuous-pumping stages. Tables 1 and 2 show our plans for the pumping tests at the Pengtsuo and Dajou sites, respectively.

We conducted resistivity-monitoring surveys during the entire pumping test at the Pengtsuo site but only during the continuous-pumping stage at the Dajou site. Fig. 3a and b show the variations of the groundwater level during the pumping test at the Pengtsuo site and the corresponding variations in the continuous-pumping stage at the Dajou site. The background groundwater levels in the P1 well at the Pengtsuo site and the PD-1 well at the Dajou site are −5.998 m and −1.700 m, respectively. Fig. 2 shows the configurations for our ERI surveys at the two sites. To reduce the noise and minimize the influence of near-surface objects, we chose the Schlumberger Array for our ERI surveys and avoided the survey line when passing through the work area where the generators and electrical cables had been installed. The survey line was 50-m long at the Pengtsuo site and 29.25-m long at the Dajou site. While conducting the surveys, we kept the line a proper

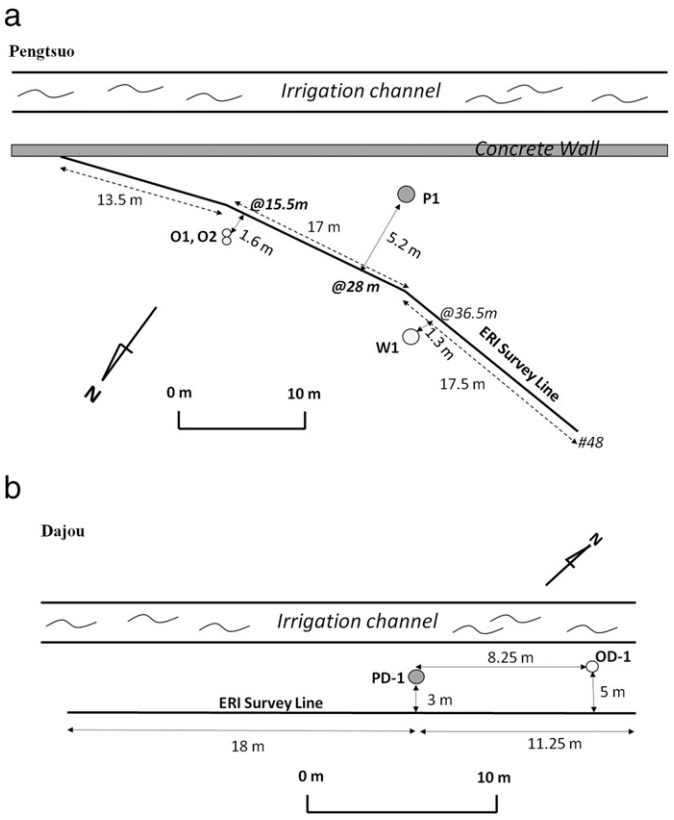

Fig. 2. The field configurations of the pumping test and the electrical resistivity imaging (ERI) survey at (a) the Pengtsuo site and (b) the Dajou site.

distance of at least 1.5 m from the well heads in order to reduce the possibility that the steel well casing would degrade our resistivity measurements. We used the LGM 4-point Light 10 W resistivity meter and the ActEle system (Lippmann, 2005) for the field-resistivity measurements. For the ERI surveys at the two sites, we chose an electrode interval of 1 m and 0.75 m. We collected measurements in the background phase of the Pengtsuo test, and conducted the ERI measurements every 40 to 60 min, depending on the quality of each survey's data. At the Dajou site, we collected ERI measurements every 10 min during the continuous-pumping stage, and measured the

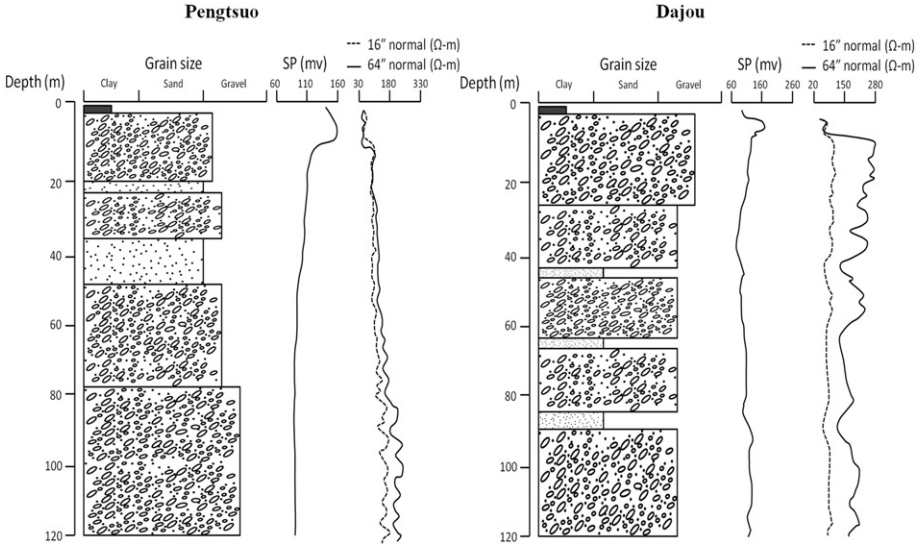

Fig. 1. The drilling core and logging records of (a) the O1 well at the Pengtsuo site and (b) the OD-1 well at the Dajou site.

Table 1
The design for the pumping test at the Pengtsuo site.

Phase	Pumping rate (m^3/h)	Duration time (min)
Background[a]	0	4315
Stepwise 1st-stage pumping	83.15	100
Stepwise 2nd-stage pumping[b]	117.41	266
Stepwise 3rd-stage pumping	Increased from 145.63 to 205.95	512
Recovery	0	529
Continuous	205.95	2902

[a] The average groundwater level is −5.998 m.
[b] Owing to a short circuit in the generator, the pumping during the second test stopped for 155 min.

background data in the recovery stage. Resistivity data were inverted with EarthImager™ 2D software (AGI, 2006), which employs iterative finite-element algorithms of forward simulation and inversion schemes to estimate subsurface resistivity structures. As suggested by Dahlin and Zhou (2004), we used the robust inversion scheme, which minimizes L1 norms and improves results in noisy environments. Furthermore, we fixed the inversion parameters so that they would complement the data-based difference inversions from various time periods relative to the background data.

3. Error analysis and depth of investigation

Labrecque et al. (1996) proposed that errors from reciprocal measurements can represent noise levels better than those errors from repeated measurements. Unfortunately we did not have enough time to collect such information during the dynamic pumping-test experiment. We made repeated measurements only during the background stages. The repeated RMS errors are 11.62% at the Pengtsuo site and 2.24% at the Dajou site (Table 3). The average RMS errors for the time-lapse difference inversions are about 10.13% at the Pengtsuo site and 0.73% at the Dajou site.

The much higher RMS errors at Pengtsuo may be due chiefly to our use of two dimensional (2D) inversion schemes for three-dimensional (3D) objects, our use of incorrect geometric factors for the bent survey line, and field noises from pumping activities. We have set up three blocky drawdown models to examine the influences that the aforementioned factors have on the difference inversions. The background model consists of a 1-m-thick, 1000 Ohm-m unsaturated layer overlying a 100 Ohm-m saturated layer. We have used two types of blocky models (Fig. 4): a 2D model with a rectangular depression cone in the saturated layer, and two 3D drawdown models (one with a straight survey line and the other with a bent survey line passing adjacent to the cubic depression cone). The depression cone has the same 1000 Ohm-m value as the unsaturated zone. We applied the forward modeling to the 2D drawdown model, and inverted the simulated measurements with 2D difference inversion relative to the simulated background measurements. We also generated the measurement responses of the 3D models, and then inverted the simulated responses with a 2D

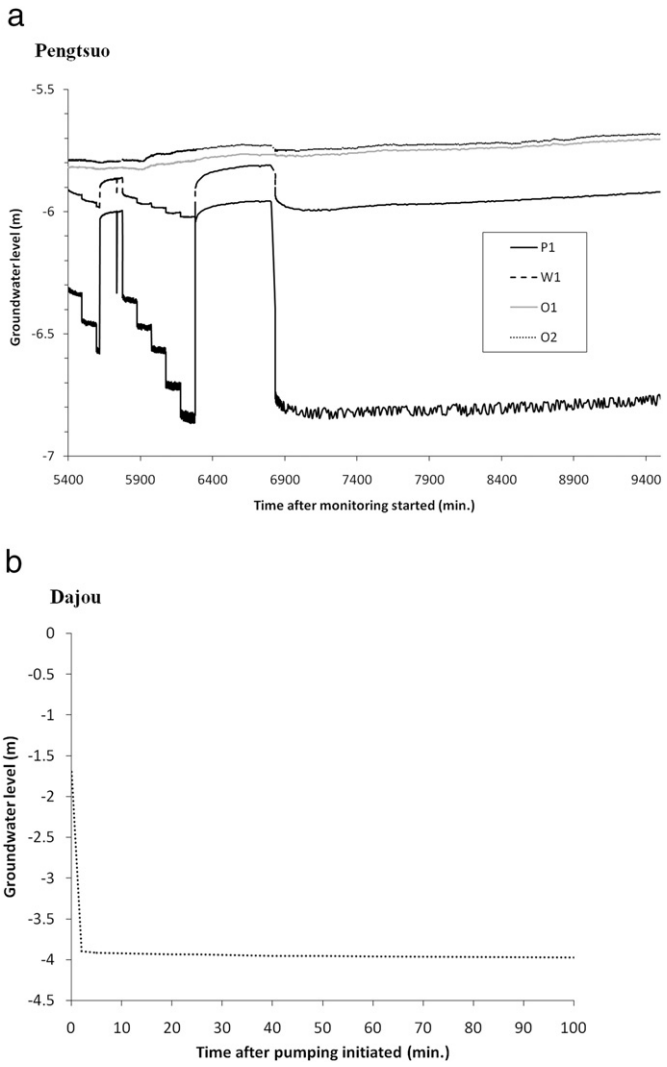

Fig. 3. (a) The records of the groundwater level registered in different wells during the pumping test at the Pengtsuo site. We started to record the background groundwater level before the pumping tests at 0 min. The pumping tests were initiated at 5394 min. (b) The groundwater level recorded at the Dajou site in the PD-1 well during the continuous-pumping test.

difference-inversion scheme. A 3% random error was applied to the forward modeling in all cases. Fig. 5 presents the inverted-percent-difference images of the 2D model and those of the 3D models. The RMS errors for the inversions of the 2D model, the 3D straight-line model, and the 3D bent-line model are 1.02%, 7.5%, and 13.74%, respectively. The RMS errors for the inversions of the two 3D background

Table 2
The design for the pumping test at the Dajou site.

Phase	Pumping rate (m^3/h)	Duration time (min)
Background[a]	0	1440
Stepwise 1st-stage pumping	103.00	100
Stepwise 2nd-stage pumping	138.20	100
Stepwise 3rd-stage pumping	169.20	100
Stepwise 4th-stage pumping	205.90	100
Stepwise 5th-stage pumping	241.50	100
Recovery	0	1440
Continuous[b]	241.50	1440

[a] The average groundwater level is −1.700 m.
[b] We conducted the resistivity monitoring only in the continuous phase.

Table 3
ERI monitoring and inversion parameters.

Array type	Pengtsuo site	Dajou site
	Schlumberger	Schlumberger
Electrode spacing (m)	1.00	0.75
Length of the profile (m)	48.0	28.5
Data points	1152	494
Average time needed per measurement (min.)	45	9
Repeated error of the background measurements (%)	11.62	2.24
RMS error of the inversion of background measurements (%)	19.85	2.71
Average RMS error of the time-lapse inversions (%)[a]	10.13	0.73

[a] Difference-inversion schemes were applied.

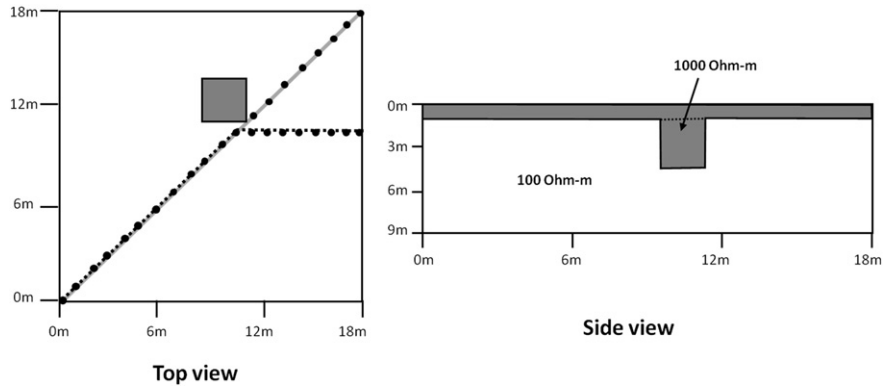

Fig. 4. The top and side view of the 3D depression-cone model. The background model consists of a 1-m-thick, 1000 Ohm-m unsaturated layer overlying a 100 Ohm-m saturated layer. The bent and straight survey lines are shown in the top view as the dotted black line and solid grey line, respectively. A resistive cubic cone of depression with a resistivity of 1000 Ohm-m is adjacent to the survey lines. The 2D model is based on the side-view model.

models are much higher than the random error (3%) we gave to the forward simulations. Although the RMS errors are high in the individual background inversions, the results of the difference inversions (as shown in Fig. 5) establish that the difference-inversion scheme can reduce the RMS errors. Indeed, in all three cases, we can resolve the resistive drawdown cone in the percent-difference images. We also found that the difference inversion of the bent-line case still has the highest RMS error (5.10%) among the three cases. Hence we have concluded that the high RMS errors for the inversions in our study come chiefly from the bent-line geometry used to map the 3D objects.

The techniques for estimating the depth of investigation (DOI) include the resolution matrix analysis (e.g., Alumbaugh and Newman, 2000; Friedel, 2003; Oldenborger and Routh, 2009), the sensitivity matrix analysis (e.g., Robert et al., 2012), and the DOI Index (e.g., Oldenborger and Routh, 2009; Oldenburg and Li, 1999). In the current study, we have adopted the procedures suggested by Caterina et al. (2013) for the appraisal of the DOI. In addition, we have explored the issue of relative model sensitivity by using EarthImager™ 2D software (AGI, 2006). Robert et al. (2012) used the sensitivity value for indicating the likely DOI, and concluded that the sensitivity value of 0.1 can better reflect their DOI in comparison to the logging data. Although the sensitivity indicator may vary in different cases, here we first use the sensitivity value of 0.1 as a quick guide for DOI for the cases discussed in Fig. 5. We found that both the 3D straight-line case and the 3D bent-line case have a shallower DOI than the 2D case. The DOI in the 3D cases are about half the DOI in the 2D case, although the difference images of the 3D

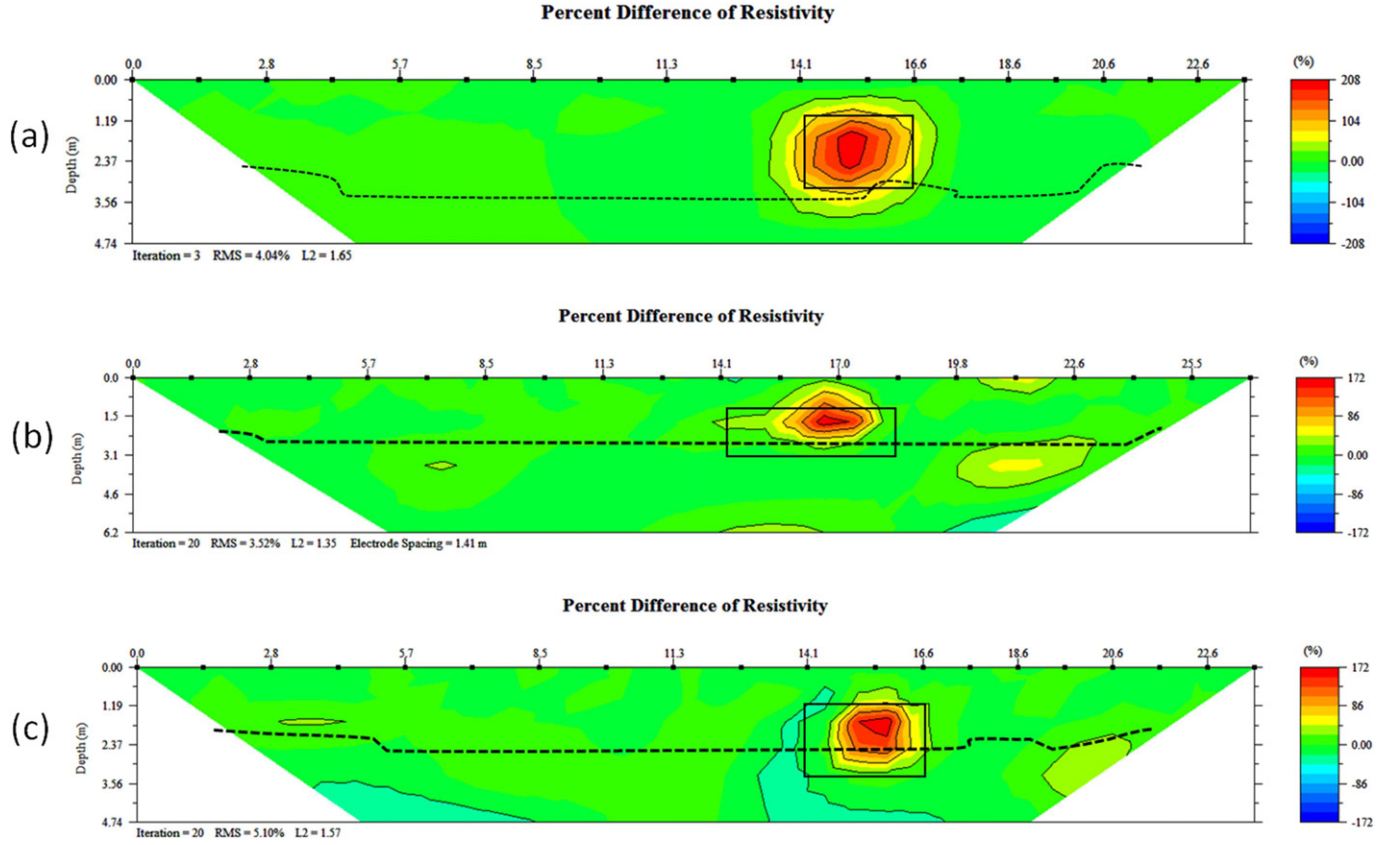

Fig. 5. The inverted-percent-difference images of (a) the 2D model, (b) the 3D model with the straight survey line, and (c) the 3D model with the bent survey line. For the background model, we inverted the images by using the 2D difference inversions combined with the robust inversion scheme. The boxes show the projected locations of the depression cone in the images, and the dotted line shows the depth of the relative sensitivity of 0.1.

cases still resolve the depressive cone. This fact implies that the DOI calculation with the 2D inversion may underestimate the actual DOI for the 3D targets when the relative sensitivity cut-off value is 0.1. Therefore, in our subsequent time-lapse difference studies at the Pengtsuo and Dajou sites, we used DOIs that are twice as deep as the depths associated with the 0.1 cut-off value.

Other factors that can generate noisy measurements in pumping environments include long measurement times in dynamic environments, induction in the ground associated with powerlines, direct current injection associated with cathodic grounding (Corwin and Hoover, 1979), and the metallic casing of a piezometer (Revil et al., 2012). These factors may have contributed to the significant repeated errors in our ERI measurements at the Pengtsuo site. After carefully arranging the array setup and avoiding interference factors as much as possible, we substantially reduced both the repeated errors and the inversion RMS errors for our measurements at the Dajou site, as shown in Table 3.

4. Results of the time-lapse ERI surveys

Archie (1942) suggested that the relationships between the in-situ resistivity of a sedimentary rock to its porosity and pore-water resistivity can be described as follows:

$$\rho_b = a{\cdot}\rho_w{\cdot}\varnothing^{-m}{\cdot}S_w^{-n}, \quad (1)$$

where ρ_b is the bulk resistivity, a is the tortuosity factor, ρ_w is the pore-water resistivity, $\varnothing$ represents the porosity, S_w is the saturation (equal to 1 when saturated), m represents the cementation exponent relative to the rock, and n denotes the saturation exponent (usually close to 2). After the pumping started, the difference between the pumping-stage images and saturated-background images within the range of the drawdown cone is reflected in the following equation:

$$\Delta\rho_b = a{\cdot}\rho_w{\cdot}\varnothing^{-m}{\cdot}\left(S_{wu}^{-n}-1\right), \quad (2)$$

where S_{wu} is the saturation corresponding to the drained soils. For the same rock or soil, one can reasonably assume that a, ρ_w, $\varnothing$, and m will remain the same after the water starts to drain from matrix pores in the pumping test. Therefore, we could find a specific resistivity-difference value at the saturation point corresponding to the air entry pressure in a relatively homogeneous media. And hence, it would be reasonable for us to delineate the groundwater surface within the drawdown cone of the pumping by using the time-lapse resistivity difference from the ERI measurements.

Fig. 6a and b show the averaged resistivity background before the pumping started for the Pengtsuo and Dajou sites. Fig. 6a presents splayed structures of low resistivity near the well locations of O1, O2, and W1. The low-resistivity structures likely indicate the influence that the wells' steel casing had on the resistivity measurements presented in Fig. 6a. By contrast, we found scant evidence of a similar well effect in Fig. 6b. Fig. 7a through f show the selected images of resistivity differences at time slices during the stepwise phases regarding the pre-pumping background measurements at the Pengtsuo site. We noted that the generator had been malfunctioning during this period, and thus, we excluded the affected images from Fig. 7. We observed that an anomalous region of increased resistivity appeared between 20 m and 35 m from the distance mark on the survey line 40 min after the pumping test had started. The anomalous region is at a depth of about 4 m on the 27.5-m mark on the survey line. Compared with the recorded groundwater levels in wells P1 and W1, the anomalous regions of increased resistivity likely corresponded to the pumping drawdown. However, the center of the anomalous region is located in the vadose zone above the groundwater surface, and because the relationship between the suction head and the water content of unsaturated soil follows non-linear curves for different types of soil, it is reasonable to conclude that a slight change of suction can significantly change water content in the vadose zone. Hence, our findings suggest that pumping may introduce a huge change in water content and a significant resistivity change in vadose zones.

Fig. 7g through i present the resistivity-difference images collected during the continuous-pumping stage at the Pengtsuo site. We noticed that the anomalous-resistivity region was exhibiting a distribution pattern different from that in the stepwise pumping. In addition, the maximum increase in resistivity increase exceeded 2000 Ohm-m during the stepwise pumping but was only about 600–1200 Ohm-m during the continuous-pumping stage. The center of the maximum-resistivity increase was at about the 27-m mark at a depth of 4 m, which is similar

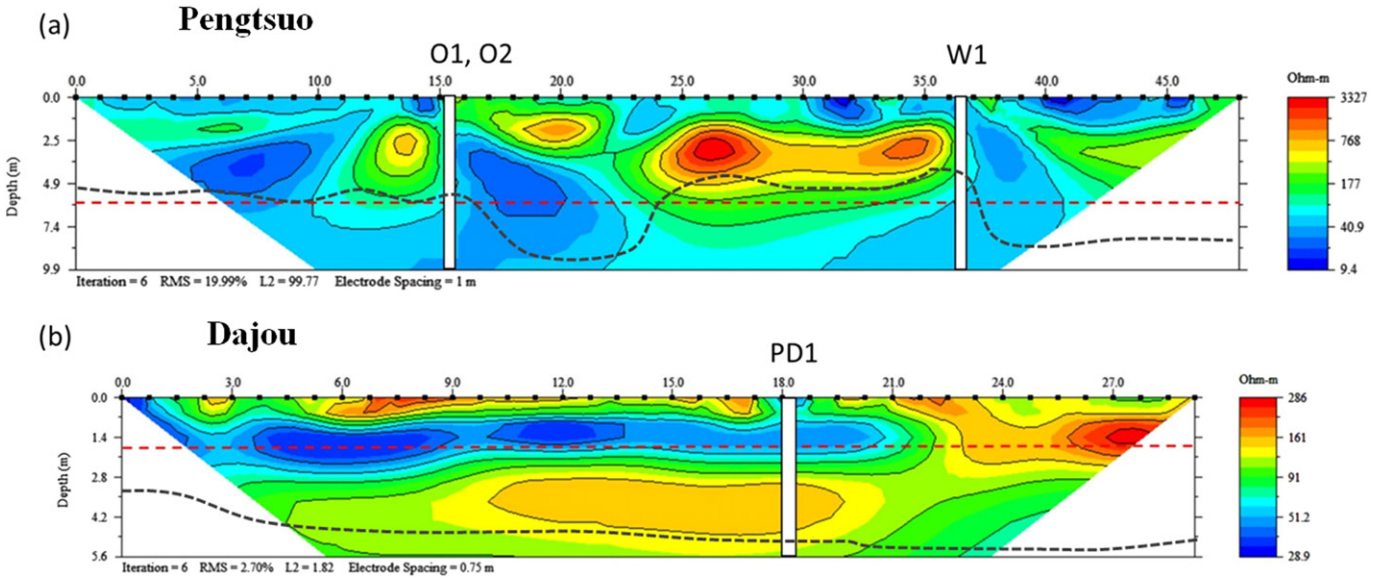

Fig. 6. The inverted resistivity image of the pre-pumping background at (a) the Pengtsuo site and (b) the Dajou site. The pumping and observation wells are shown at the projected positions on the survey line. The dotted red lines indicate the groundwater surface. And the black dash line shows the modified likely depth of investigation, which is double the depth of the relative sensitivity of 0.1.

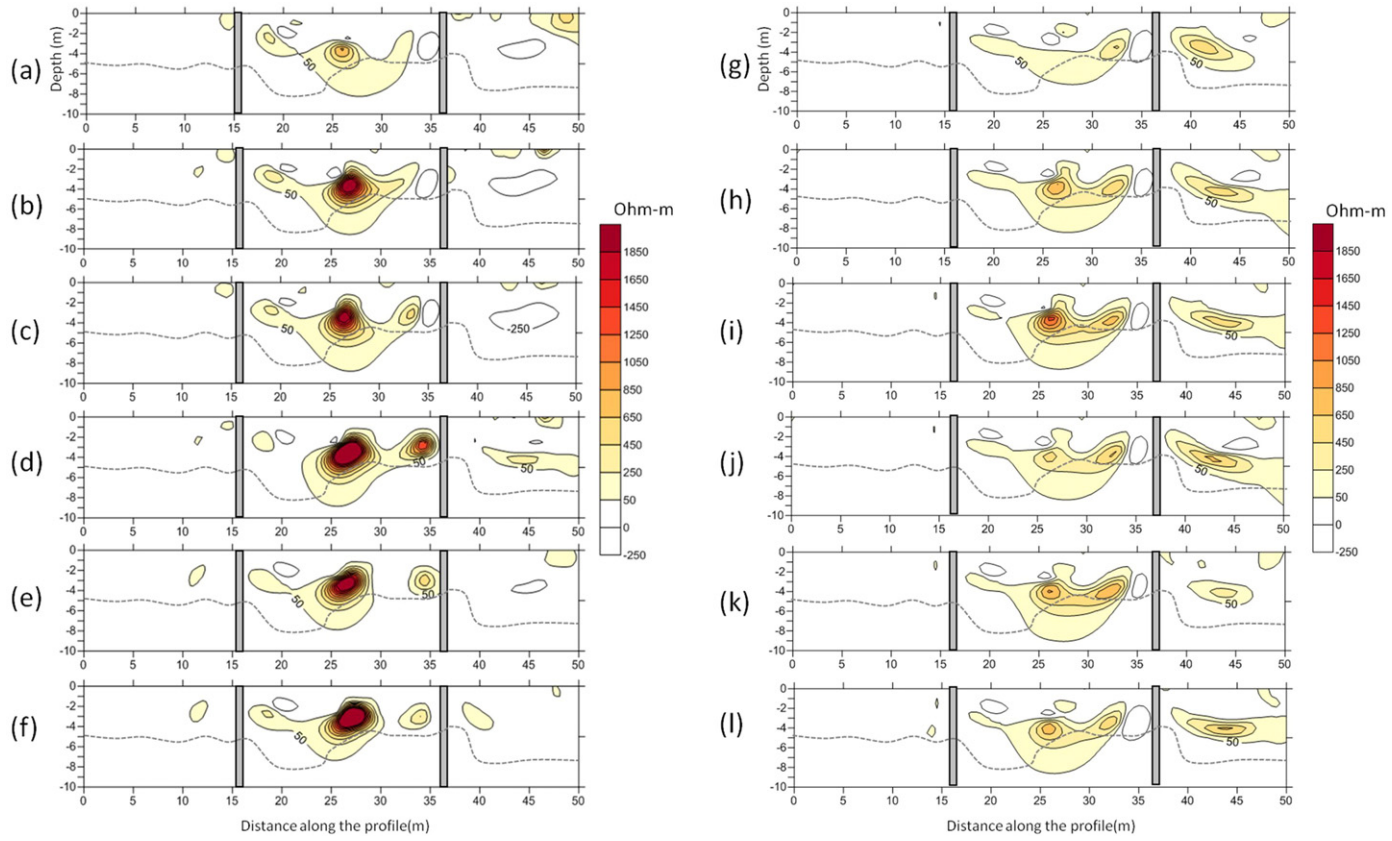

Fig. 7. The selected resistivity-difference images collected at (a) 83 min., (b) 128 min., (c) 178 min., (d) 542 min., (e) 662 min., and (f) 702 min. After the start of pumping during the stepwise-pumping phase, and at (g) 39 min., (h) 291 min., (i) 401 min., (j) 451 min., (k) 676 min., and (l) 766 min. After the start of pumping during the continuous-pumping phase at the Pengtsuo site. The dashed line shows the modified depth of investigation, which is double the depth of the relative sensitivity of 0.1.

to the anomaly during the stepwise pumping. In contrast to the images of the stepwise pumping, an additional anomalous region appeared between the 40-m and 45-m mark in the vadose zone during the continuous-pumping stage. The region can be seen in Fig. 7d but is absent from the other images of stepwise pumping.

Fig. 8 shows the resistivity-difference images regarding the pre-pumping background during the first 120 min of the continuous-pumping stage at the Dajou site. Each image indicates the measurements taken every 10 min. We found that there is no significant anomaly corresponding directly to the drawdown cone, as shown in Fig. 8a through e. In the first 50 min of pumping, the regions of resistivity increase were only in the vadose zone above a depth of 1.7 m. As shown in Fig. 8f, a region with a resistivity increase higher than 1.6 Ohm-m appeared at a depth of 2 m to 4 m between 20 m and 25 m from the distance mark near the pumping well. After 70 min of pumping, we discovered a clear cone-shaped anomalous region near the pumping well, as shown in Fig. 8f. And as shown in Fig. 8e, the maximum increase in the region's resistivity was over 2.8 Ohm-m at a depth of about 1.7 m, which corresponds to the groundwater surface before pumping. From 70 to 120 min after pumping started, the anomalous resistivity region remained about the same size but the maximum resistivity difference increased from about 2.8 Ohm-m to over 4.4 Ohm-m in Fig. 8g through i. The findings suggest that the drawdown cone seems to have remained the same size but that the saturation status within the cone varied during the period. In addition, we found that the well caused a “blank” area 18 m from the distance mark, as shown in the difference images in Fig. 8f through i, although we observed no significant well effect in the background images for the Dajou site.

5. Discussion

When we compared groundwater-level records with resistivity differences, we found that the groundwater surface correlated roughly to resistivity increases of 140 Ohm-m and 100 Ohm-m during the stepwise-pumping phase and the continuous-pumping phase, respectively. Regarding Archie's law, we attempted to delineate the contour line corresponding to resistivity of 140 Ohm-m below a depth of 6 m (the pre-pumping groundwater level), which might clarify the geometric variation of the drawdown cone during the pumping activity. Fig. 9a shows the contour line's spatial variations corresponding to a resistivity value of 140 Ohm-m at the end of the three stages of the stepwise-pumping phase and 100 Ohm-m in the continuous-pumping phase. In Fig. 9a, the concave region enclosed by the 140-Ohm-m contour line got larger and its center was at the 26.5-m mark in the first and second stages of the stepwise-pumping phase. The pumping rate increased gradually to a maximum rate of 205.95 cm h during the third stage of the stepwise-pumping phase, and the region enclosed by the 140-Ohm-m contour line during the third stage grew larger than did the same region during the second stage of the stepwise-pumping test. In addition, the center of the region slightly moved to the 25.5-m mark during the third stage. The increased space of the concave region may reflect the enlarged drawdown cone associated with the increasing pumping rate. In addition, we found that the center of the drawdown cone shifted about a meter during the period extending from the second stage to the third stage of the stepwise-pumping test. Two possible factors might help explain the cone's shifting center: first, the aquifer perhaps had heterogeneity regions when the drawdown cone grew larger and encountered these regions at the third stage of the

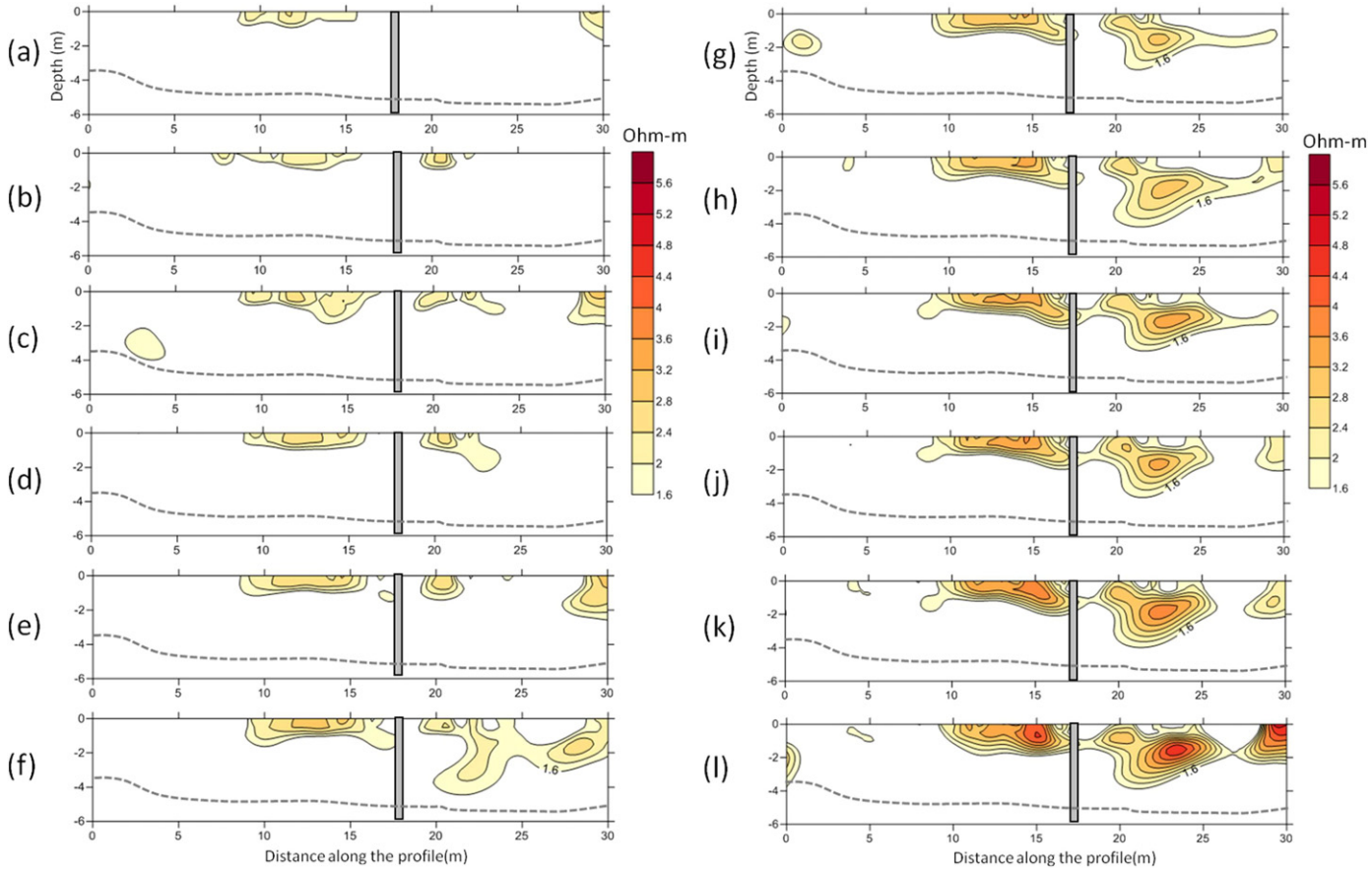

Fig. 8. The resistivity-difference images collected at (a) 10 min., (b) 20 min., (c) 30 min., (d) 40 min., (e) 50 min., (f) 60 min., (g) 70 min., (h) 80 min., (i) 90 min., (j) 100 min., (k) 110 min., and (l) 120 min. After the start of pumping during the continuous-pumping phase at the Dajou site. The dashed line shows the modified depth of investigation, which is double the depth of the relative sensitivity of 0.1.

stepwise-pumping phase; and second, the effluent water was drained into the nearby irrigation channel and may have leaked back into the aquifer via the channel, hence distorting the shape of the cone.

We found that the post-pumping increase in resistivity at the Dajou site was far smaller than the corresponding increase at the Pengtsuo site. When we compared the resistivity-difference images with the water-level records in the PD-1 well, we found that the groundwater level roughly correlated to a resistivity increase of 1.6 Ohm-m. Fig. 9b shows the 1.6-Ohm-m isoline of resistivity difference regarding the pre-pumping measurements below a depth of 2 m after 120 min of continuous pumping at the Dajou site. The center of the drawdown cone is at about the 22-m distance mark and close to the pumping well PD-1. Unfortunately, the well-casing effect might have masked some small variation of resistivity near the well. Therefore, we could not delineate the shape of the drawdown cone for the regions near PD-1.

We used both the drawdown cone's geometry and the distance-drawdown method provided by Halford and Kuniansky (2002) to estimate hydraulic conductivity by Eq. (3), assuming that the resistivity difference contour between the pumping phases and background can represent the geometries of the groundwater surface. In Eq. (3),

$$K = \frac{Q}{\pi} \frac{\ln\left(\frac{r_2}{r_1}\right)}{h_2^2 - h_1^2}, \tag{3}$$

Q is the pumping rate, h_1 is the head at distance r_1 from the center of the drawdown cone, and h_2 is the head at distance r_2 from the center of the drawdown cone (Fetter, 2001).

To calculate the specific yield (S_y), we attempted to use the resistivity image that we had taken right after initiating the pumping test. And to this end, we used the ratio of total pumped-water volume to the estimated drawdown-cone volume calculated from the resistivity measurements:

$$S_y = \frac{Q \cdot \Delta t}{V_d}, \tag{4}$$

where Δt is the pumping time and V_d is the drained volume. Using only the measurements from the first drawdown-cone image after the start of continuous pumping, we tried to minimize the influence that the lateral recharge's extra water volume could have on the estimation of drained water volume. This extra water may still have caused over-estimations of specific yields, and hence our estimation should be viewed only as the "upper bound" of the given specific yield.

Table 4 shows the calculated hydraulic conductivity for the Pengtsuo site. The estimated hydraulic conductivities increased from 2.50×10^{-5} to 6.33×10^{-5} m/s in the stepwise-pumping phase, and were about 1.33×10^{-4} m/s in the continuous-pumping phase at the Pengtsuo site. It seems that the estimated hydraulic conductivity increased with the increasing pumping rate. The values are close to those calculated from the measured groundwater-level variations in multiple wells (about 9.65×10^{-5} m/s). In addition, the estimated specific yield was about 0.12, and turned out to be close to the value calculated from the time-drawdown analysis (about 0.13).

Table 5 reveals our estimates of hydraulic conductivity and specific yield from the continuous-pumping test at the Dajou site. The estimated hydraulic conductivity was about 2.50×10^{-4} m/s, and this value turns out to be about a quarter of the values calculated in the multiple-well

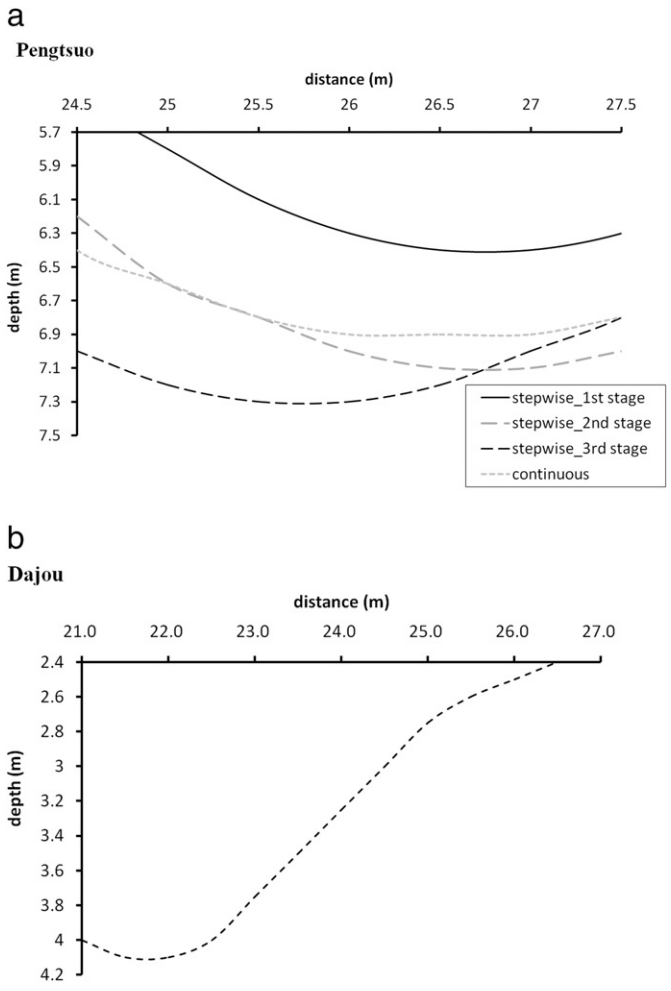

Fig. 9. (a) The estimated groundwater surface within the depression cone during the stepwise- and continuous-pumping phases at the Pengtsuo site. (b) The estimated groundwater surface in the depression cone during the continuous-pumping phase at the Dajou site.

time-drawdown analysis (about 1.00×10^{-3} m/s). In addition, the depression cone appeared after 60 min of pumping at the Dajou site. The findings suggest that the drawdown cone either was very small or was kept near the pumping well, which was a distance of 3 m from the survey line in the first 50 min. Therefore, we could not detect the drained region of the depression cone in these resistivity measurements. We assume that the drawdown was due to the additional water that had drained between the 50th minute and the 60th minute of pumping. The estimated specific yield, about 0.22, agrees well with the value calculated from the multiple-well time-drawdown analysis (about 0.19).

Comparing Table 4 to Table 5, we can see that the calculated hydraulic conductivity of the Dajou site from the time-drawdown analysis was about 10 times the hydraulic conductivity of the Pengtsuo site. And from the resistivity measurements, we can see that the estimated hydraulic conductivity of the Dajou site was about twice the value of the Pengtsuo site. The much larger hydraulic conductivity at the Dajou site suggests that the pumping's drained water at this site may, in general, stem chiefly from quick lateral recharge, not from the in-situ water in pores near the pumping well. As a result, the depression cone appeared only after 60 min of pumping at the Dajou site. Neuman (1987) proposed that, to account for lateral radial flow, the estimations of specific yields in Eq. (3) should undergo the following modification:

$$S_y = F\frac{Q\cdot\Delta t}{V_d}, \tag{5}$$

Table 4
The hydraulic parameters from the time-drawdown calculation in previous tests at the Pengtsuo site and the estimated parameters from the time-lapse resistivity measurements in this study.

	K(m/s)	Sy
Previous test in O1	9.75E-05	0.13
Previous test in O2	9.54E-05	
Stepwise 1st-stage	2.50E-05	
Stepwise 2nd-stage	3.50E-05	
Stepwise 3rd-stage	6.33E-05	
Continuous	1.33E-04	0.12

Table 5
The hydraulic parameters from the time-drawdown calculation at the Dajou site in the previous tests and the estimated parameters from the time-lapse resistivity measurements in this study.

	K(m/s)	Sy
Previous test in Dajou1	1.66E−05	0.17
Previous test in Dajou2	1.70E−05	0.19
Continuous	4.16E−06	0.22

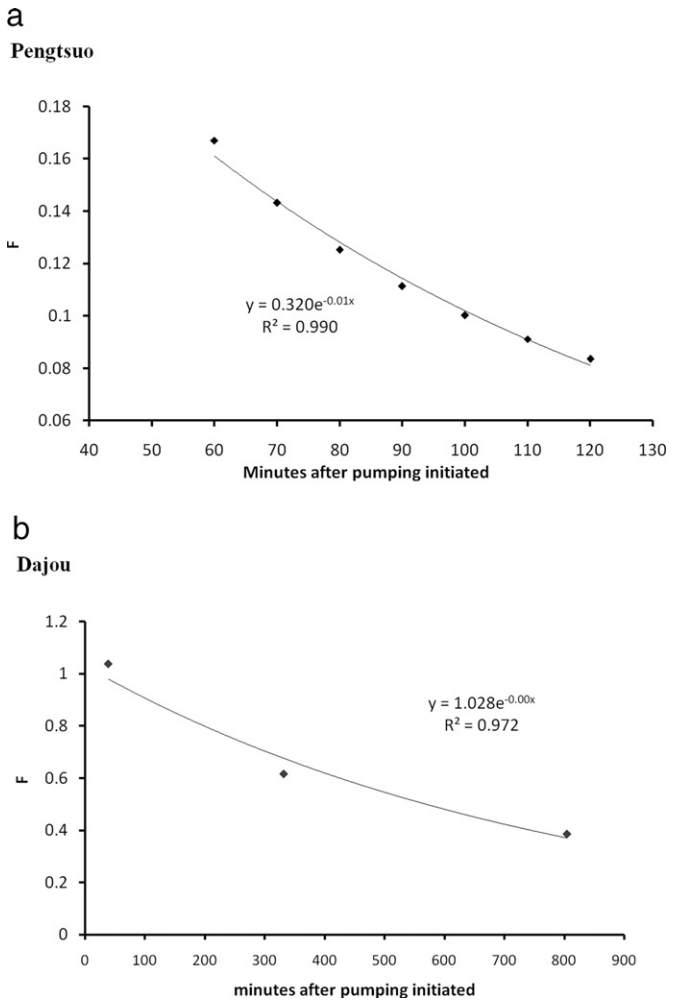

Fig. 10. (a) The changes in the estimated fraction (F) that represent the ratio of the storage yields caused by the falling water table to the total pumping discharge during the continuous-pumping test at the Dajou site. (The solid line is the regression curve based on the assumption of exponential decreases.) (b) The variations of fraction F at the Pengtsuo site. The solid line represents the regression curve based on the assumption of exponential decreases.

where F represents the fraction of the instantaneous discharge rate coming from the storage yielded by the falling depression cone. If we calculate that the Dajou site's specific yield (S_y) is 0.22, we can estimate the fraction F at different times during the continuous-pumping phase, as shown in Fig. 10a. Fig. 10a suggests that the fraction of instantaneous discharge released from storage by the falling groundwater table decreased exponentially with time, and that about 70% of the discharge water came from lateral flow right after the start of pumping. The lateral-flow groundwater took over 90% of the pumping discharge after 100 min of pumping at the Dajou site. If the specific yield of the Pengtsuo site was 0.12, we can account for almost 100% of the pumping discharge, which was from the storage yielded by falling water levels. The ratio of instantaneous storage yield to pumping discharge dropped slowly to about 0.6 after 320 min of pumping, and to about 0.4 after 800 min of pumping. The contribution of the lateral flow right after the pumping started also re-affirms the assertion that the hydraulic conductivity at the Dajou site is, in general, much larger than that at the Pengtsuo site.

6. Conclusions

In this study, we used time-lapse electrical-resistivity measurements to estimate hydraulic conductivity and specific yields during pumping tests at the Pengtsuo and Dajou test sites. We inverted the resistivity data with the difference inversions relative to the background measurements, and used the resistivity-difference images to estimate the relevant parameters. The average RMS errors for the time-lapse difference inversions are about 10.13% and 0.73% for the measurements at the Pengtsuo and Dajou sites, respectively. We built three depression cone models, including one 2D model and two 3D models (the first 3D model having a straight survey line and the second having a bent survey line). Then we inverted the simulated resistivity measurements from the three models to examine possible noise and other artifacts in our field measurements. From the modeling, we concluded that the higher RMS inversion errors of the Pengtsuo data may majorly come from the geometry of the bent survey line. Although the bent-line case may yield a higher RMS error than the straight-line one, we found that the difference inversion can still resolve the depression cone.

Drawing on Archie's law, we assumed that the resistivity differences between the data collected during pumping and the data for the pre-pumping background would exhibit a change in water content because of dewatering during pumping activity. We compared the resistivity difference with the groundwater-level records registered at the pumping tests, and selected the resistivity difference that best represents the depression cone's groundwater surface. We used the distance-drawdown calculations to estimate the hydraulic conductivity of the unconfined aquifer from the resistivity results during different pumping stages. We also estimated the specific yield of the same unconfined aquifer by dividing the pumping volume by the volume of the drawdown cone at the start of pumping. The estimated hydraulic conductivity and the specific yield of the gravel-unconfined aquifer were about 1.33×10^{-4} m/s and 0.12 at the Pengtsuo site, and about 2.50×10^{-4} m/s and 0.22 at the Dajou site. These values agree with the parameters that we calculated in our multiple-well time-drawdown analysis at the Pengtsuo site (about 9.65×10^{-5} m/s and 0.13) and at the Dajou site (about 1.00×10^{-3} m/s and 0.19).

Using a modified calculation proposed by Neuman (1987), we estimated the contribution that the lateral flow made to the pumping discharge. Also according to our findings, about 100% of total pumping discharge is from the instantaneous storage yield at the Pengtsuo site. Furthermore, the ratio of storage yield to pumping discharge dropped slowly from about 100% to about 0.4 after 800 min of pumping. By contrast, about 70% of the discharged water came from the lateral flow that occurred right after the pumping started at the Dajou site. The lateral-flow groundwater provided over 90% of the pumped discharge after the first 100 min of pumping at the Dajou site. The contribution of the lateral flow to the pumping discharge right after the start of pumping also confirms that the hydraulic conductivity at the Dajou site was much larger than that at the Pengtsuo site.

Acknowledgement

The study was funded by the Central Geological Survey (control number 104-5226904000-04-01), MOEA, R.O.C. We are grateful for the help from the pumping-test engineers at Taiwan Sugar Company. The important data used in the manuscript are listed in the tables and figures, and further detailed data can be accessed by email (pingyuc@gmail.com).

References

AGI, 2006. Instruction Manual for EarthImager 2D Ver. 2.3.0. Advanced Geosciences, Inc., Austin, Texas.
Alumbaugh, D.L., Newman, G.A., 2000. Image appraisal for 2-D and 3-D electromagnetic inversion. Geophysics 65, 1455–1467.
Archie, G.E., 1942. The electrical resistivity log as an aid in determining some reservoir characteristics. Pet. Trans. AIME 146, 54–62.
Barker, R., Moore, J., 1998. The application of time-lapse electrical tomography in groundwater studies. Lead. Edge 18, 1454–1458.
Bevan, M.J., Endres, A.L., Rudolph, D.L., Parkin, G., 2003. The non-invasive characterization of pumping-induced dewatering using ground penetrating radar. J. Hydrol. 218, 55–69.
Binley, A., Cassiani, G., Middleton, R., Winship, P., 2002. Vadose zone flow model parameterisation using cross-borehole radar and resistivity imaging. J. Hydrol. 267, 147–159.
Caterina, D., Beaujean, J., Robert, T., Nguyen, F., 2013. A comparison study of different image appraisal tools for electrical resistivity tomography. Near Surf. Geophys. 11, 639–657.
Chang, P.-Y., Chang, S.-K., Liu, H.-C., Wang, S.C., 2011. Using integrated 2D and 3D resistivity imaging methods for illustrating the mud-fluid conduits of the Wushanting mud volcanoes in southwestern Taiwan. Terr. Atmos. Ocean. Sci. 22, 1–14.
Cooper, H.H., Jacob, C.E., 1946. A generalized graphical method for evaluating formation constants and summarizing well field history. Trans. Am. Geophys. Union 27, 526–534.
Corwin, R.F., Hoover, D.B., 1979. The self-potential method in geothermal exploration. Geophysics 44, 226–245.
Dahlin, T., Zhou, B., 2004. A numerical comparison of 2D resistivity imaging with 10 electrode arrays. Geophys. Prospect. 52, 379–398.
Endres, A.L., Clement, W.P., Rudolph, D.L., 2000. Ground penetrating radar imaging of an aquifer during a pumping test. Ground Water 38, 566–576.
Fetter, C.W., 2001. Applied Hydrogeology. 4th ed. Prentice Hall.
Friedel, S., 2003. Resolution, stability and efficiency of resistivity tomography estimated from a generalized inverse approach. Geophys. J. Int. 153, 305–316.
Halford, K.J., Kuniansky, E.L., 2002. Documentation of Spreadsheets for the Analysis of Aquifer-Test and Slug-Test Data.
Kemna, A., Kulessa, B., Vereecken, H., 2002. Imaging and characterisation of subsurface solute transport using electrical resistivity tomography (ERT) and equivalent transport models. J. Hydrol. 267, 125–146.
Kim, J.-H., Yi, M.-J., Song, Y., Cho, S.-J., Chung, S.-H., Kim, K.-S., 2002. DC resistivity survey to image faults beneath a riverbed. 15th EEGS Symposium on the Application of Geophysics to Engineering and Environmental Problems.
Labrecque, D.J., Miletto, M., Daily, D., Ramirez, A., Owen, E., 1996. The effects of noises on Occam's inversion of resistivity tomography data. Geophysics 61, 538–548.
Leven, C., Dietrich, P., 2006. What information can we get from pumping tests? Comparing pumping test configurations using sensitivity coefficients. J. Hydrol. 319, 199–215.
Lippmann, E., 2005. Four-Point Light Hp Technical Data and Operating Instructions Ver. 3.37. Lipmann Geophysikalische Messgeräte, Schaufling, Germany.
Loke, M.H., Chambers, J.E., Rucker, D.F., Kuras, O., Wilkinson, P.B., 2013. Recent developments in the direct-current geoelectrical imaging method. J. Appl. Geophys. 95, 135–156.
Mitchell, N., Nyquist, J.E., Toran, L., Rosenberry, D.O., Mikochik, J.S., 2008. Electrical resistivity as a tool for identifying geologic heterogeneities which control seepage at Mirror Lake, Nh. 21st EEGS Symposium on the Application of Geophysics to Engineering and Environmental Problems.
Neuman, S.P., 1987. On methods of determining the specific yield. Ground Water 25 (6), 679–684.
Oldenborger, G.A., Routh, P.S., 2009. The point-spread function measure of resolution for the 3-D electrical resistivity experiment. Geophys. J. Int. 176, 405–414.
Oldenburg, D.W., Li, Y., 1999. Estimating depth of investigation in DC resistivity and IP surveys. Geophysics 64, 403–416.
Revil, A., Karaoulis, M., Johnson, T., Kemna, A., 2012. Review: some low-frequency electrical methods for subsurface characterization and monitoring in hydrogeology. Hydrogeol. J. 20, 617–658.

Rizzo, E., Suski, B., Revil, A., Straface, S., Troisi, S., 2004. Self-potential signals associated with pumping tests experiments. J. Geophys. Res. Solid Earth 109.
Robert, T., Caterina, D., Deceuster, J., Kaufmann, O., Nguyen, F., 2012. A salt tracer test monitored with surface ERT to detect preferential flow and transport paths in fractured/karstified limestones. Geophysics 77, B55–B67.
Straface, S., Fallico, C., Troisi, S., Rizzo, E., Revil, A., 2007. An inverse procedure to estimate transmissivity from heads and SP signals. Ground Water 45, 420–428.
Theis, C.V., 1935. The relation between the lowering of the piezometric surface and the rate and duration of discharge of a well using groundwater storage. Trans. Am. Geophys. Union 16, 519–524.
Toran, L., Johnson, M., Nyquist, J., Rosenberry, D., 2010. Delineating a road salt plume in lakebed sediments using electrical resistivity, piezometers, and seepage meters at Mirror Lake, NH. Geophysics 75, 73–85.
van Schoor, M., 2002. Detection of sinkholes using 2D electrical resistivity imaging. J. Appl. Geophys. 50, 393–399.